



# Fatigue analysis of additively manufactured short carbon fiber-reinforced PETG Components

Mithila Rajeshirke<sup>1</sup> · Suhas Alkunte<sup>1</sup> · Orkhan Huseynov<sup>1</sup> · Ismail Fidan<sup>2</sup>

Received: 24 April 2023 / Accepted: 1 August 2023 / Published online: 7 August 2023  
© The Author(s), under exclusive licence to Springer-Verlag London Ltd., part of Springer Nature 2023

## Abstract

The aim of this study is to conduct processing and fatigue analysis on components made from short carbon fiber-reinforced Polyethylene Terephthalate Glycol (SCF-PETG) using the Material Extrusion (MEX) method. For this study, commercially available SCF-PETG filament and filament developed in the laboratory with different carbon fiber weight percentages are studied under constant stress conditions to verify the effect of parametric conditions, i.e., type of laminates (unidirectional, angle-ply, and cross-ply), layer heights (0.3, 0.2, 0.1, and 0.05 mm), and carbon fiber weight percentages (13.78%, 10% and 16%). The Kruskal–Wallis test is performed to analyze the experimental data. It was observed that fatigue life is greatly affected by varying process parameters. The S–N curve is also obtained by testing specimens at four stress levels with optimized printing parameters. An optical microscope was used to study fiber orientation and fiber length for the filament which is extruded in the laboratory. After fatigue testing, scanning electron microscopy (SEM) is performed to observe the microstructure of the specimens fractured under fatigue loading. The findings of this study could prove to be highly beneficial in the production of fiber-reinforced composites that exhibit enhanced overall properties suitable for application in the automotive, aerospace, and robotics field.

**Keywords** Short carbon fiber · Material extrusion · Fatigue analysis · Composite material · PETG

## 1 Introduction

Additive manufacturing (AM) is a multifaceted, state-of-the-art manufacturing technology that produces prototypes or functional components. As opposed to conventional manufacturing processes that create leftovers and waste, AM technology does not generate waste except for support materials

in the case of complex designs. There are seven major AM processes which are direct energy deposition (DED), binder jetting (BJT), powder bed fusion (PBF), MEX, sheet lamination (SHL), material jetting (MJT), and vat photopolymerisation (VPP) [1–3]. MEX is a commonly used and widely adopted additive manufacturing (AM) technology that goes by multiple names, including fused filament fabrication (FFF) or fused deposition modeling (FDM) in certain research studies. MEX produces three-dimensional objects through the extrusion of semi-molten thermoplastic materials from a heated nozzle or nozzles onto a platform. A range of polymeric materials including epoxy, nylon, polyester, PETG, acrylonitrile butadiene styrene (ABS), polycarbonate (PC), polylactide (PLA), and polyamide (PA) can be utilized in the MEX process [4].

MEX offers several benefits, including the ability to produce complex parts, low cost, minimal material wastage, design flexibility, customization of products for individual consumers, and production of small lots of parts [5]. Along with these, contrary to conventional manufacturing technologies, MEX does not require jigs, fixtures, molds, and post-processing processes such as drilling. Even with all

---

✉ Ismail Fidan  
ifidan@tntech.edu

Mithila Rajeshirke  
mcrjeshir42@tntech.edu

Suhas Alkunte  
ssalkunte42@tntech.edu

Orkhan Huseynov  
ohuseynov42@tntech.edu

<sup>1</sup> Department of Mechanical Engineering, College of Engineering, Tennessee Tech University, Cookeville, TN 38505, USA

<sup>2</sup> Department of Manufacturing and Engineering Technology, College of Engineering, Tennessee Tech University, Cookeville, TN 38505, USA

these benefits of MEX, the lack of mechanical properties is the primary concern of polymer parts in industrial applications. So, its applications as functional components are limited. Various studies have focused on MEX techniques with single thermoplastic materials [6–9]. The limitations of single-polymer parts produced by MEX render them unsuitable for applications that demand high mechanical strength. In response to this need, fiber-reinforced additive manufacturing (FRAM) technology has emerged. Recently FRAM has widened the scope of the thermoplastic polymers in AM as their unique properties such as lower melting temperature, tailorable mechanical properties, subsequent formability, and, very importantly, the ability to easily incorporate additives into the base polymers play a vital role [10]. FRAM enables researchers to investigate a wider range of material possibilities by combining different matrix and fiber materials, as well as varying the form of the fibers. FRAM not only combines the advantages of AM and composite materials but also provides ease in the production of complex parts over the conventional manufacturing processes of composites. Figure 1 depicts a schematic view of FRAM for SCF composites.

Advancements in FRAM have made it possible to use polymeric structures in a range of load-bearing and structural applications. However, cyclic loading can result in fatigue, causing structural damage and eventual catastrophic failure at lower stress levels than those seen with normal mechanical loading. Cyclic loading refers to the repeated application of stress or strain on a material over time. Unlike normal mechanical loading, where a material is subjected to a constant or static load, cyclic loading causes unique challenges and can result in fatigue failure. Because cyclic loading causes fatigue in materials due to fluctuations in stress levels, microstructural changes, and the initiation and

propagation of cracks. Stress concentration, strain localization, reduced fracture toughness, creep, residual stresses, and environmental effects further contribute to cumulative damage. As a result, cyclic loading can lead to catastrophic failure at stress levels lower than those observed under normal mechanical loading conditions. Therefore, it is of utmost importance to investigate the fatigue behavior of composite parts produced via FRAM. Fatigue testing is conducted under various loading conditions, including tension, compression, torsion, or bending. In more complex fatigue analyses, combinations of these conditions are used. The most straightforward stress sequence in fatigue testing involves a constant stress amplitude, where all cycles are identical, as illustrated in Fig. 2. The figure also shows the notation for testing parameters under constant amplitude

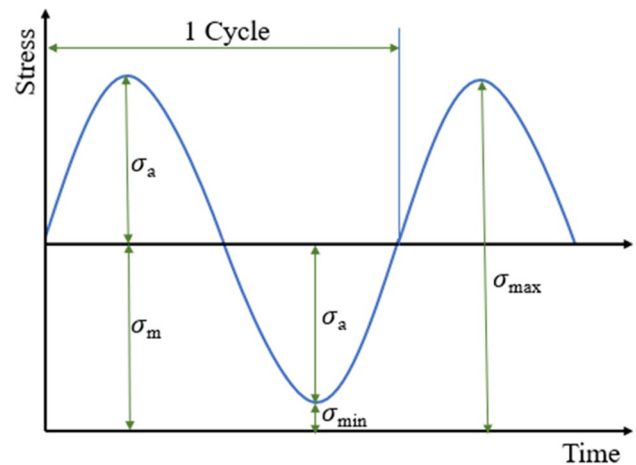
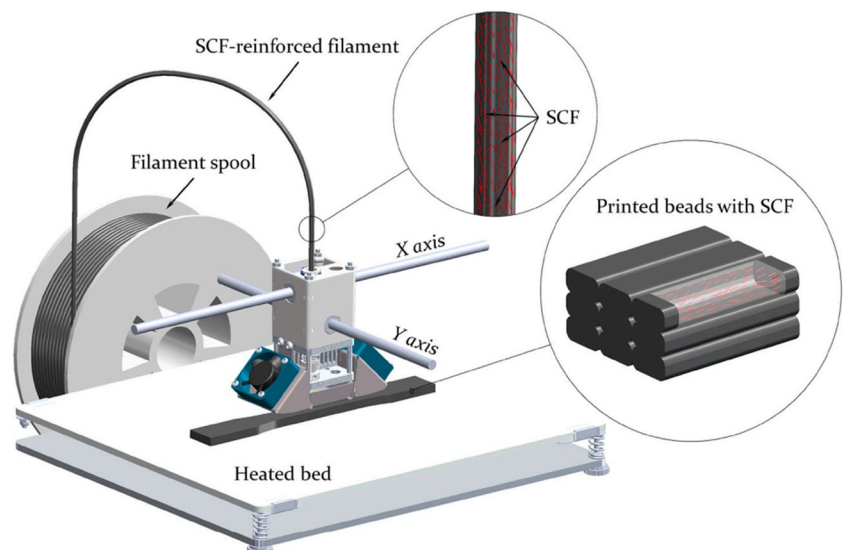


**Fig. 2** The notation for testing parameters under constant amplitude loading

**Fig. 1** Schematic view of the FRAM process [11]

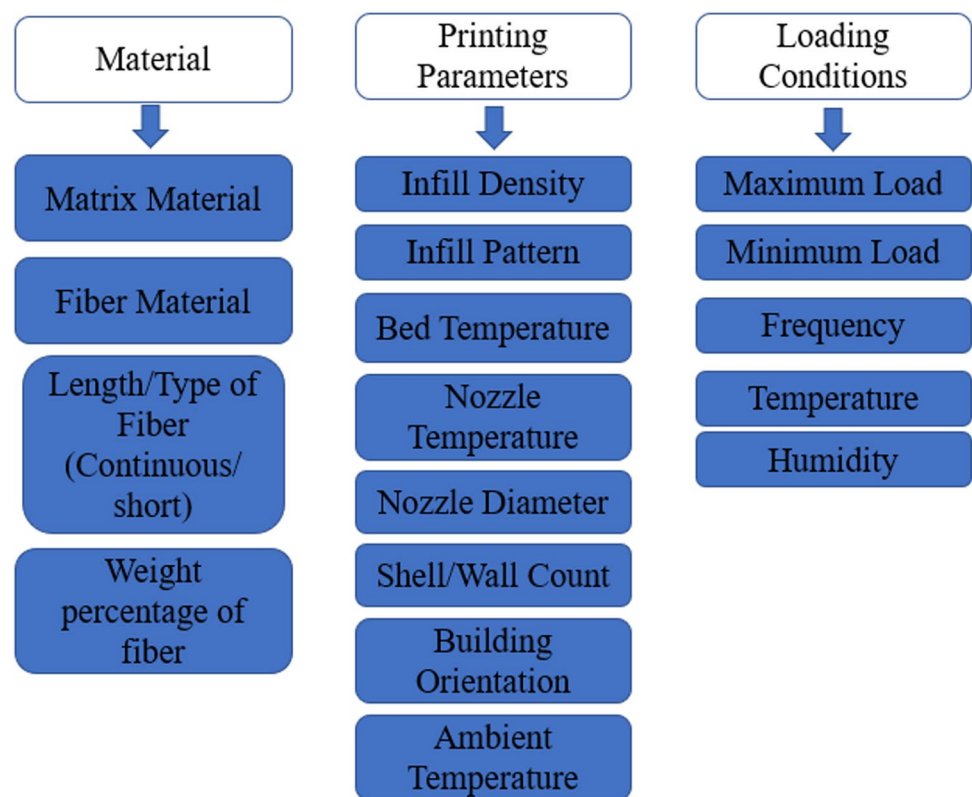


loading. The alternating stress, mean stress, maximum stress, and minimum stress in each cycle are denoted by  $\sigma_a$ ,  $\sigma_m$ ,  $\sigma_{max}$ , and  $\sigma_{min}$ , respectively. The stress ratio is expressed as  $R = \sigma_{min}/\sigma_{max}$ . The mechanical properties of composites can be influenced by several parameters, as revealed by the literature review [12]. These parameters include the fiber material, matrix material, volume or weight percentage of fiber in the matrix, fiber type and length, as well as printing process parameters such as infill pattern, build orientation, infill density, layer height, printing speed, printing plane, nozzle diameter, bed temperature, etc. [1, 13, 14]. Figure 3 shows the parameters affecting the fatigue life of any fiber-reinforced composites. The following sections discuss various fatigue behavioral research studies on single polymers and continuous fiber-reinforced composites.

As previously stated, numerous studies have focused on investigating individual thermoplastic polymers' static and fatigue properties. Andrzejewska et al. [15] focused on the tensile and fatigue properties of PLA specimens manufactured by FFF and injection molding. Researchers considered the parameters of infill density, fiber orientation, and infill pattern. Comparing the tensile and fatigue strength properties, it was found that injection-molded specimens exhibited higher values than their 3D-printed counterparts. In their study, Dolzyk et al. [7] conducted a uniaxial fatigue test on PETG material that was 3D printed via FDM. The testing was performed at four different raster directions (0°, 90°,

45°, and crosshatched 45°/-45°) and at stress levels of 90%, 80%, 70%, and 60% of the ultimate tensile strength (UTS). The PETG samples that were printed in the longitudinal orientation exhibited the longest fatigue life at the 90% of UTS, according to the study. The samples also showed reduced anisotropic properties, likely due to stronger inter-layer bonding. He et al. [6] conducted a study in which they investigated the bending fatigue behavior of FDM-manufactured ABS beams under various thermomechanical loading conditions and printing parameters, including building orientation, nozzle diameter, and layer thickness. The results showed that the specimens printed with a building orientation of 0°, filament width of 0.8 mm, and layer thickness of 0.15 mm exhibited the longest vibration time before fracturing at each temperature. Additionally, the study found that a larger nozzle size and thicker layer height could increase the fatigue life of the specimens. Padzi et al. [8] conducted a study in which they compared the fatigue properties of ABS specimens produced through FDM and molding processes under various loading conditions. The findings showed that the fatigue life of the 3D-printed part was lower. Additionally, Afrose et al. [9] investigated the fatigue behavior of FDM-processed PLA material under various loading conditions. They examined the effect of part builds' orientation (x, y, and 45°) on the material's fatigue strength when tested at different percentages of the ultimate tensile stress nominal value. The results showed that the parts built at a 45°

**Fig. 3** Parameters affecting the fatigue life of AM components



orientation exhibited longer fatigue life compared to those built in the X and Y orientations. This finding was surprising since all the parts were subjected to the same percentage of static loads.

As mentioned in the following section, many researchers have studied the fatigue behavior of continuous fiber-reinforced composites. Imeri et al. [16, 17] have evaluated the effect of different fiber materials (Kevlar, carbon fiber, and fiberglass), fiber pattern (concentric and isotropic), and infill type on the tension-tension fatigue properties of FRAM specimens with a load ratio of 0.1. The study concluded that carbon fiber had better fatigue resistance than other reinforcing materials. Adding more rings improves fatigue life for concentric infill, while for isotropic infill, it weakens the fatigue performance. Pertuz-Comas et al. [18] presented research on fatigue bending tests on continuous fiber-reinforced composites manufactured by the FFF technique at various loading conditions. The matrix material was Onyx, with 19% continuous Kevlar fiber as reinforcement. The experimental data obtained were fitted with Basquin's model. Based on the value of parameter  $b$  of Basquin's equation, the composite is concluded as brittle. Giannakis et al. [19] investigated continuous CF-Nylon composites' tensile and fatigue properties, and the S–N curve was fitted. It has been concluded that nylon served only as a matrix and did not play a crucial role in fatigue life. Nylon, PLA, and CF-Nylon are also compared under tensile loading. In their investigation, Alberto D. Pertuz et al. [20] presented the tensile and fatigue behavior of nylon and continuous fiber-reinforced nylon, considering factors such as infill pattern, infill density, different fibers, and printing orientations. The experimental results indicated that the specimens reinforced with carbon fiber and printed in the  $0^\circ$  orientation exhibited a higher number of cycles before failure. Moreover, among the specimens with concentric ring reinforcement, the configuration with 2 rings and 4 layers showed better fatigue response compared to the one with 4 rings and 2 layers.

Likewise, researchers have also reported on the various composites manufactured by MEX/FDM/FFF. In their study, Travieso-Rodriguez et al. [21] explored the fatigue properties of PLA-wood composites manufactured through FDM with a range of parameters. These parameters include varying nozzle diameters (0.7, 0.6, and 0.5 mm), layer heights (0.2, 0.3, and 0.4 mm), infill patterns (rectilinear and honeycomb), infill densities (25, 50, and 75%), and extrusion velocities (25, 30, and 35 mm/s), with a fixed 8% wood fiber reinforcement. A rotating bending fatigue test was conducted, revealing that the fatigue strength of the PLA-wood fiber composite was lower than that of pure PLA. This was attributed to inadequate fiber-matrix adhesion and an increase in void formation. The study reported that the ideal FDM printing parameters for achieving the highest number of cycles to failure were a honeycomb filling pattern, a

nozzle diameter of 0.7 mm, a layer height of 0.4 mm, and a filling density of 75%. In their study, Essassi et al. [22] examined the fatigue characteristics of sandwich composites made from PLA and flax fibers through cyclic bending tests. The composites were created with different densities of the auxetic core. Results indicated that the sandwich composites with a lower core density of 8.3% exhibited a longer fatigue life. Anouar EL MAGRI et al. [23] have presented the Quasi-static tensile and tension-tension fatigue behavior along with the self-heating phenomenon of PLA-Graphene material manufactured by FFF. This research examines the impact of varying print speed, platform temperature, and frequencies on fatigue lifetime. The findings indicate that the mentioned process parameters have a significant influence on fatigue lifetime. Additionally, the results show that when the frequency is 80 Hz, the coupling effect of thermal and mechanical fatigue leads to a decrease in fatigue lifetime due to self-heating. Moreover, the mechanical properties of woven continuous carbon fiber composites were compared to those of two nonwoven AM printed composites (unidirectional and multidirectional fibers), where the fibers were continuous and discontinuous both. Emmanuel J. Ekoi et al. [24] conducted tests on the tensile, flexural, and fatigue properties of these materials. For the fatigue testing, unidirectional continuous fiber reinforced specimens and woven CF specimens were tested at 50, 70, and 100% loading levels of respective tensile strengths. Upon testing, it was found that 70% of woven carbon composites outperformed unidirectional (nonwoven) carbon fiber composites.

There are few studies presenting the fatigue behavior of short-fiber reinforced composites. Results of 3-point bending tests for short Kevlar-reinforced epoxy composites produced through direct write 3D printing were presented by Nawafleh et al. [25]. The tests were conducted under static and dynamic (fatigue) loading conditions. The fatigue strength of composites reinforced with Kevlar fibers at a medium volume level (3.5%) was found to be greater than that of composites reinforced with the highest level (6.3%) of Kevlar fibers. This variation in reinforcement percentage was investigated and reported in the study. Capela et al. [26] have presented their work on short carbon fiber-reinforced epoxy composites with different carbon fiber volume fractions manufactured by molding. It was concluded that the strength increases for both static and fatigue tests until the fiber volume fraction reaches 17.5%, after which it remains relatively constant.

Based on the survey of existing literature, it is apparent that significant research has been conducted on the fatigue characteristics of both individual thermoplastic polymers and continuously reinforced fiber composites. Some of the researchers reported on the fatigue behavior of composites reinforced with short and discontinuous fibers but not with the MEX technique. The type of laminate, layer height, and

carbon fiber weight percentage are potentially vital factors that can affect the fatigue life of the composite components. As far as the author is aware, no research has specifically examined these factors and their impacts on SCF-PETG composites produced via the FRAM technique. In our proposed work, commercially available SCF-PETG filament and filament developed in the laboratory with different carbon fiber weight percentages are studied under constant loading conditions to verify the parametric conditions, i.e., type of laminate, layer height, and SCF weight percentage. The S–N curve is also obtained by testing specimens with optimized printing parameters under different stress conditions. Finally, fractographic analysis is performed to observe the microstructure after breaking the specimens under fatigue loading.

## 2 Materials and methods

### 2.1 Material

An amorphous PETG has excellent mechanical properties, including high impact resistance, tensile strength, and flexural strength [27, 28]. PETG has a relatively high glass transition temperature ( $T_g$ ) of around 80 °C [29], which means it can withstand high temperatures without losing its structural integrity. PETG is easy to print on MEX printers due to its low shrinkage and minimal warping [30, 31]. It offers high strength over low cost compared to other polymers [32]. Additionally, PETG has noticeable flexibility, high thermal resistance [33], durability [31], and excellent chemical resistance [27].

The incorporation of SCF into polymer matrices is currently being explored as a promising approach to enhancing the fatigue properties of composites. The reinforcement of SCF to PETG increases the modulus of elasticity stiffness, compressive modulus, and tensile strength of the composite [32, 34]. SCF are more malleable than continuous fibers and are also less expensive to produce, allowing them to be shaped into intricate forms. In light of the benefits of PETG and SCF, the former was chosen as the matrix and the latter as the fiber. Two types of filaments are used in this research: Commercial filament, which is available as SCF-PETG (or CF-PETG) by the manufacturer Push Plastic [35], and Custom-made filament is extruded in the laboratory with different weight percentages of SCF.

#### 2.1.1 Commercial filament

Table 1 displays the characteristics of the commercial filament as provided in the manufacturer's datasheet. In this research, as SCF weight percentage is taken as one of the process parameters, it is important to know about it. In order

**Table 1** Material properties of SCF/PETG for commercial filament [35]

Properties	Values
Tensile strength at yield	96.52 (N/mm <sup>2</sup> )
Flexural strength	141.34 (N/mm <sup>2</sup> )
Tensile elongation at break	4.00%
Specific gravity	1.31
Flexural modulus	6894.75(N/mm <sup>2</sup> )

to ascertain the weight percentage of SCF in the matrix material of the commercial filament, the filament is cut and subjected to thermogravimetric analysis (TGA) using a SDT 650 system. The SDT 650 is a Simultaneous Thermal Analyzer (STA) from TA Instruments. It is used to study the change in transitions of a polymer under conditions of controlled temperature, time, and atmosphere. The SDT 650 uses TRIOS software for instrument control, data analysis, and reporting. TGA involves burning off the matrix material PETG. TGA is a technique used to measure the changes in the mass of a sample as it is subjected to a controlled temperature program [36]. The TGA is conducted under Nitrogen atmosphere, utilizing a heating program with a temperature range of 25 °C to 786.94 °C and a ramp rate of 10 °C per minute. The analysis reveals that the weight percentage of SCF is 13.78%. Figure 4 displays TGA set up with filament before the test (a) and the remains of SCF after the test (b). Figure 5 displays the graphical representation of the TGA.

#### 2.1.2 Custom-made filament

The schematic view for extruding the filament is shown in Fig. 6. The configuration comprises a low-temperature furnace, an air path, a filament spooler, and a filament extruder equipped with a hardened steel nozzle head with a diameter of 2.85 mm. Prior to the production of filament, PETG pellets, and SCF were separately kept for drying in the low-temperature furnace/dryer to prevent the formation of bubbles caused by absorbed moisture during extrusion. These bubbles result in defects and reduce the surface quality of the filament. Then, after 6–7 h of drying, SCF is weighed on a weighing machine and then PETG pellets are added according to the selected weight ratio. Furthermore, this mixture is tumbled manually and then incorporated into the extruder. The extrusion parameters, such as air path fan speed, extrusion speed, and spooler speed, can be adjusted to achieve a uniform filament diameter. The filament extrusion parameters employed in this study are presented in Table 2. The matrix material used for filament extrusion was PETG pellets sourced from 3DXTECH [37], while the reinforcement was provided by SCF from ZOLTEK [38]. SCF has an average fiber length of 100–150 μm and a diameter of 7.2 μm.

**Fig. 4** TGA set up (a) Filament before test, (b) Remains of SCF after test

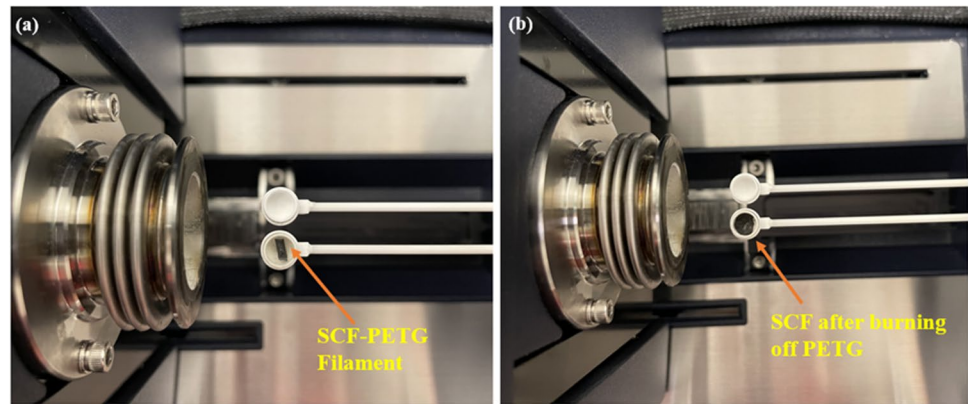
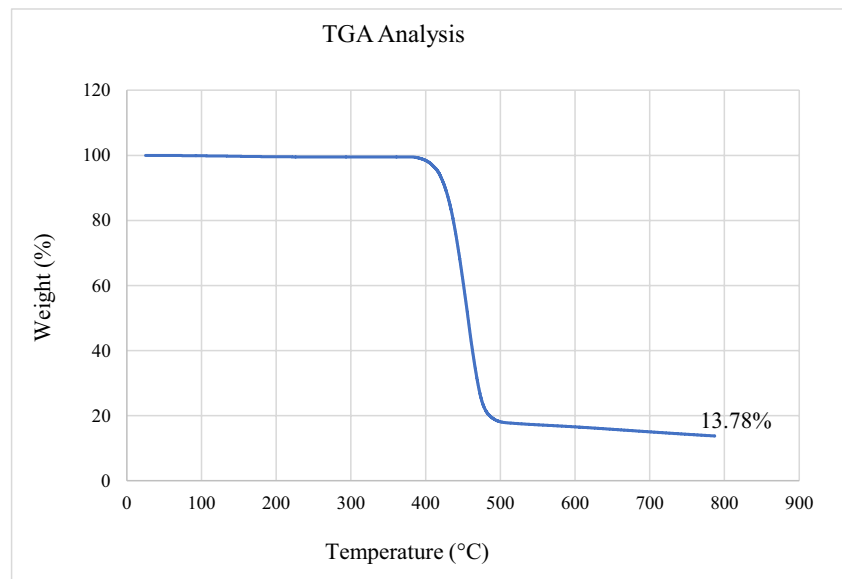


**Fig. 5** Graphical representation of the TGA for commercial filament



When the SCF-PETG is extruded for one time, specimens printed with this custom-made filament (SCF 16% weight percentage) are studied under an optical microscope, and it shows that fibers are accumulated in some places, and also those are not oriented in one direction. So, the filament is cut into small pieces and extruded a total of three times. After the third extrusion, it is visible from Figures 9 and 11, that carbon fibers are almost unidirectional or very slightly partially oriented to the printing direction, unlike the first extrusion as in Figs. 7 and 10 in which SCF are completely disoriented and randomly distributed.

Figure 7 shows a microstructure image for SCF-PETG (16% by weight) for the first extrusion of filament. Figure 8 shows the microstructure image for SCF-PETG (16% by weight) for the second extrusion of filament and Fig. 9 shows the microstructure image for SCF-PETG (16% by weight) for the last extrusion of filament. For the first extrusion, the fibers are seen as accumulated at some places, and fibers are completely disoriented. Figure 10 describes the microstructure image for fiber distribution of SCF-PETG (16% by

weight) for the first extrusion of filament. From this figure also, anomalies such as gaps at various sections are visible, and fibers are accumulated at many locations for the first extrusion samples. From Fig. 11 i.e., microstructure image for fiber distribution of SCF-PETG (16% by weight) for last extrusion of filament, the fibers seem to be well distributed and almost unidirectional or very slightly partially oriented to the printing direction. From these observations, it was decided to extrude the filament three times and then utilize it for printing the specimen required for fatigue testing.

## 2.2 Experimental set-up

The geometry is selected according to ISO 11782–1:1998(E) standard for the research as given in Fig. 12. The CAD model is produced using SOLIDWORKS and saved in STL format. The resulting STL file is then imported into the PRUSA slicing software, where printing parameters are established. The software generates G-code, which is subsequently used by the PRUSA i3 MK3 printer with a 0.4 mm

**Fig. 6** The Schematic view for extruding the filament

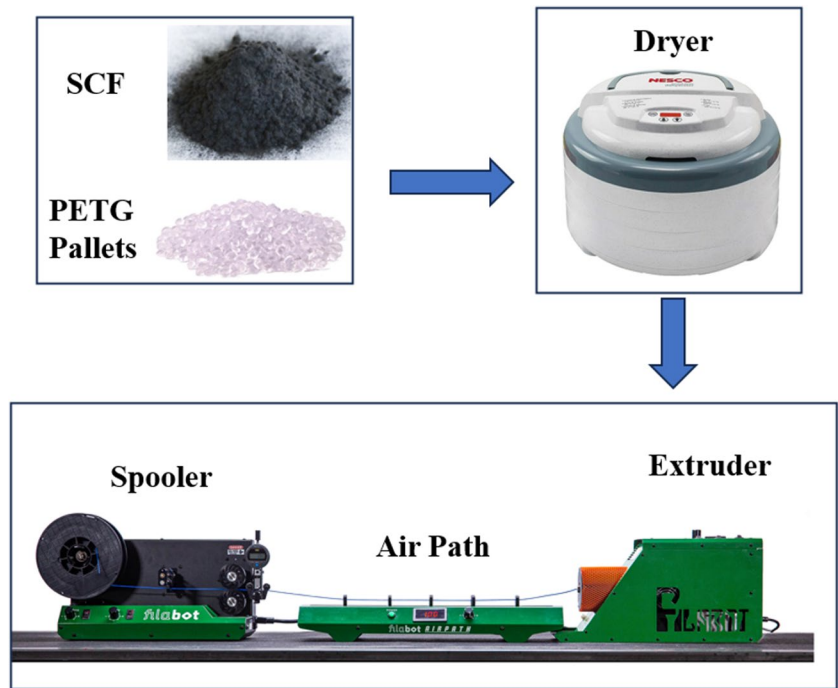


**Table 2** Processing parameters for filament extrusion

Properties	Values
Extrusion speed	25 (mm/s)
Extrusion temperature	220 (°C)
Airpath speed	50 (m/s)
Filament diameter	2.66 – 2.84 (mm)

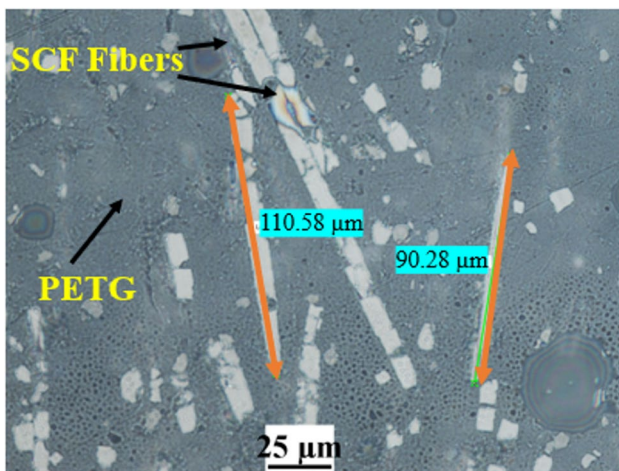


**Fig. 7** Microstructure image for SCF-PETG (16% by weight) for first extrusion of filament

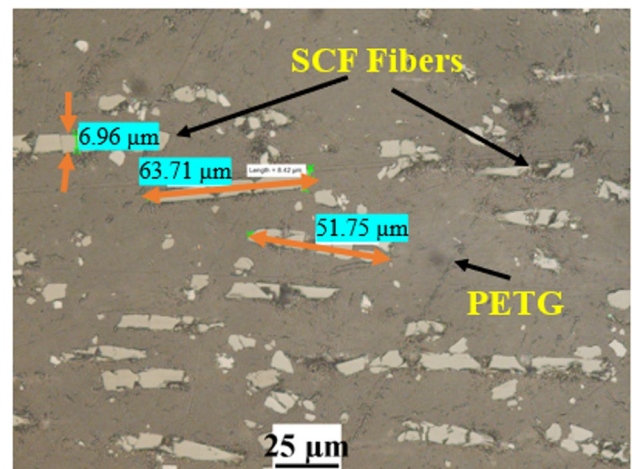


**Fig. 8** Microstructure image for SCF-PETG (16% by weight) for second extrusion of filament

diameter hardened steel nozzle. Three process parameters considered here are the type of laminates, layer heights, and

SCF weight percentages. The values of fixed printing parameters and varying parameters considered for this research work are shown in Tables 3 and 4, respectively. The printing plane (XY) and types of laminates are seen in Figs. 13(a-d).

The fatigue properties of the material are evaluated through uniaxial tensile loading in accordance with the ISO 11782–1:1998(E) standard [39]. The tests are carried out under tensile-tensile conditions with a stress ratio of 0.1. The values of maximum stress, i.e., 52 MPa, and minimum stress, i.e., 5.2 MPa, are kept uniform for all the specimens tested for parametric studies. A frequency of 3 Hz was utilized

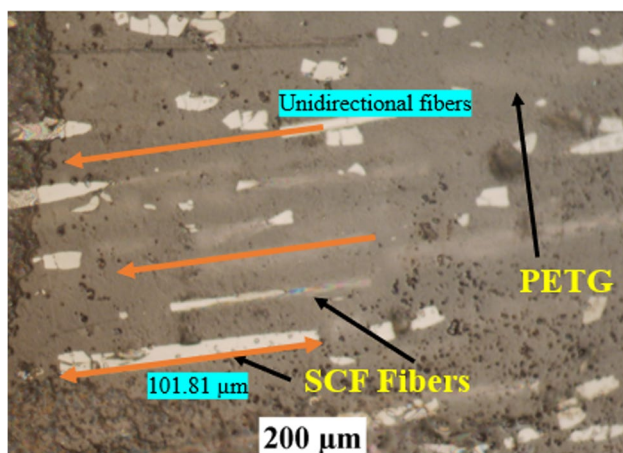


**Fig. 9** Microstructure image for SCF-PETG (16% by weight) for last extrusion of filament

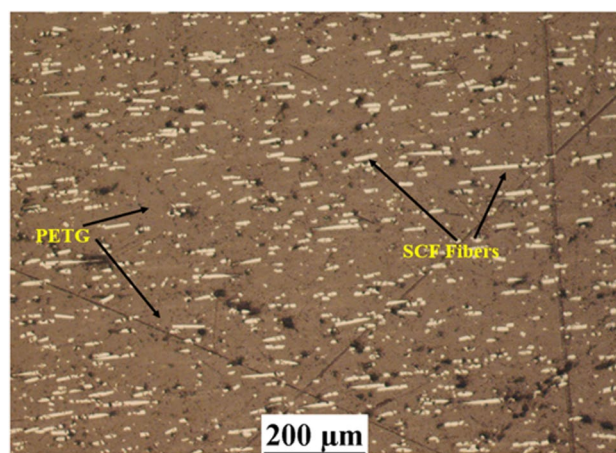


**Fig. 11** Microstructure image for fiber distribution of SCF-PETG (16% by weight) for last extrusion of filament

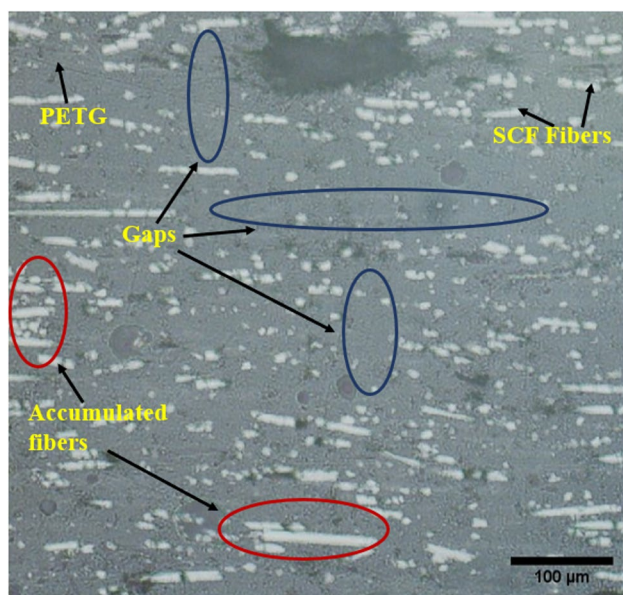


**Fig. 10** Microstructure image for fiber distribution of SCF-PETG (16% by weight) for first extrusion of filament

while conducting the tests under controlled conditions of 54–61% humidity and 19–23 °C temperature. The Newton test machine controller/software was employed to regulate the test parameters. Accurate waveform control required the configuration of Proportional/Integral/Derivative (PID) values. The PID values employed were 1100–1400 for proportional, 100 for integral, and 0 for derivative, respectively. To determine the appropriate input values for the experiments, several pilot experiments were conducted on SCF-PETG filaments. Six repetitions were tested for each level of the factor. The load-controlled fatigue test was employed, whereby the loads were regulated, and the response to the tests was documented in the form of cycle counts. 810E4-15 Dynamic

Test System and some of the fractured specimens after testing are shown in Figs. 14 (a, b), respectively. For both static and fatigue testing applications, it has the capability to withstand an axial load of 15 kN. The experiments are conducted in three stages to check the effects of the following:

1. Type of laminate: Unidirectional laminate  $[0^\circ]_{50}$ , Angle-ply laminate  $[45^\circ/-45^\circ]_{25}$ , and Cross-ply laminate  $[0^\circ/90^\circ]_{25}$ . Unidirectional laminate  $[0^\circ]_{50}$  means that all the layers, i.e., 50 layers, are printed in  $0^\circ$ , which is the direction of loading. Angle-ply laminate  $[45^\circ/-45^\circ]_{25}$  means that for every alternate layer, directions are changed from  $45^\circ$  to  $-45^\circ$ , and the number of layers is 25. Similarly, cross-ply laminate  $[0^\circ/90^\circ]_{25}$  means that for every alternate layer, directions are changed from  $0^\circ$  to  $90^\circ$ , and the number of layers is 25.
2. Layer height: 0.05, 0.1, 0.2, and 0.3 mm.
3. SCF weight percentage: 13.78% (Commercial Filament), 10% (Custom-made Filament), and 16% (Custom-made Filament).

Different types of laminates and variations in SCF weight percentage can show varying stiffness and strength. Layer height is also a key factor, as the quality and mechanical properties of MEX parts depend on it. Considering these points, the parameters are selected for this study. After getting the results for all of the above tests, the optimal parameters from the mentioned process parameters are selected to conduct further experiments to plot Stress Vs. Number of cycles (S–N graph) with Basquin's model. There are several models which are used to curve fit or basically to predict the fatigue values. However, Basquin's model is simple, and it can also be related to fiber-reinforced composites [40]. It can be represented by Eq. (1). The material constants A and b are utilized in the equation where S represents the tensile stress and  $N_f$  represents the cycles to failure.



**Fig. 12** Specimen geometry according to ISO 11782–1:1998(E) standard (All dimensions are in mm)

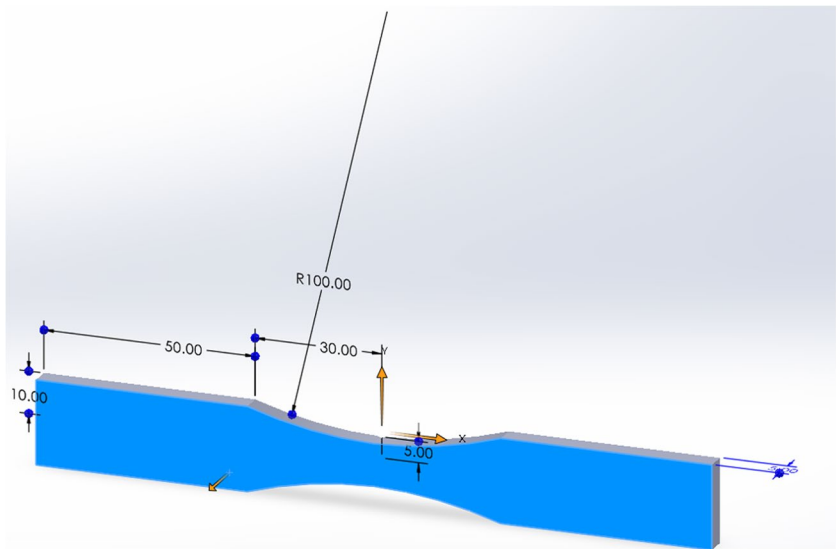


**Table 3** Fixed printing parameters

Parameters	Values
Infill density	100%
Infill pattern	Aligned rectilinear
Nozzle diameter	0.4 (mm)
Nozzle temperature	240 (°C)
Bed temperature	90 (°C)

**Table 4** Varying process parameters

Parameters	Values/Types
Layer Height	0.05, 0.1, 0.2, 0.3 (mm)
Type of Laminates	Unidirectional laminate [0°] <sub>50</sub> , Angle-ply laminate [45°/-45°] <sub>25</sub> , Cross-ply laminate [0°/90°] <sub>25</sub>
SCF weight percentage	13.78% (Commercial Filament), 10% (Custom-made Filament), 16% (Custom-made Filament)

$$S = A \cdot N_f^b \tag{1}$$

### 3 Results and discussion

#### 3.1 Effect of type of laminates

Three different types of laminates or stacking sequences are used for the study, i.e., unidirectional laminate [0°]<sub>50</sub>, angle-ply laminate [45°/-45°]<sub>25</sub>, and cross-ply laminate [0°/90°]<sub>25</sub>.

All other printing parameters, such as layer height (0.2 mm), carbon fiber percentage (Commercial Filament – 13.78%), etc., are kept constant. The tests are carried out with constant stress conditions, i.e., 52 MPa maximum stress and 5.2 MPa minimum stress. The outcome is measured in the structure of the number of cycles. The data obtained from the experimental results are shown in Table 5. The graphical representation of the results obtained is shown in Fig. 15. Statistical analysis was conducted on the fatigue results to evaluate the impact of laminates. The hypotheses were formulated as follows. The null hypothesis states that the fluctuation of laminates does not exert a noteworthy impact on fatigue properties, while the alternative hypothesis proposes that the variation of laminates has a statistical impact on fatigue properties.

To perform the statistical analysis in this investigation, Minitab was utilized for the Shapiro–Wilk normality test. Before executing the ANOVA, the normality of the data was evaluated via the Shapiro–Wilk normality test. The test result generated a p-value of 0.010 with a significance level of 0.05. Besides, it was discovered that the assumption of equal variances had been violated. Consequently, instead of ANOVA, a non-parametric test, the Kruskal–Wallis [41] method, was opted to analyze the data. Table 6 displays the Kruskal–Wallis test summary for the laminate type. The p-value denoting the distinction in the laminate type is less than 0.05. This implies substantial proof against the null hypothesis and implies a notable dissimilarity between the groups. From Fig. 15, and Table 5, it is observed that the highest number of cycles obtained is 888 for unidirectional laminate [0°]<sub>50</sub>. For angle-ply [45°/-45°]<sub>25</sub> and cross-ply laminate [0°/90°]<sub>25</sub>, there is not much dispersion, but the number of cycles sustained is very low. It can be concluded that the optimal laminate is the unidirectional laminate [0°]<sub>50</sub>.

**Fig. 13** (a) Printing plane (b) Unidirectional laminate  $[0^\circ]_{50}$  (c) Angle-ply laminate  $[45^\circ/-45^\circ]_{25}$  (d) Cross-ply laminate  $[0^\circ/90^\circ]_{25}$

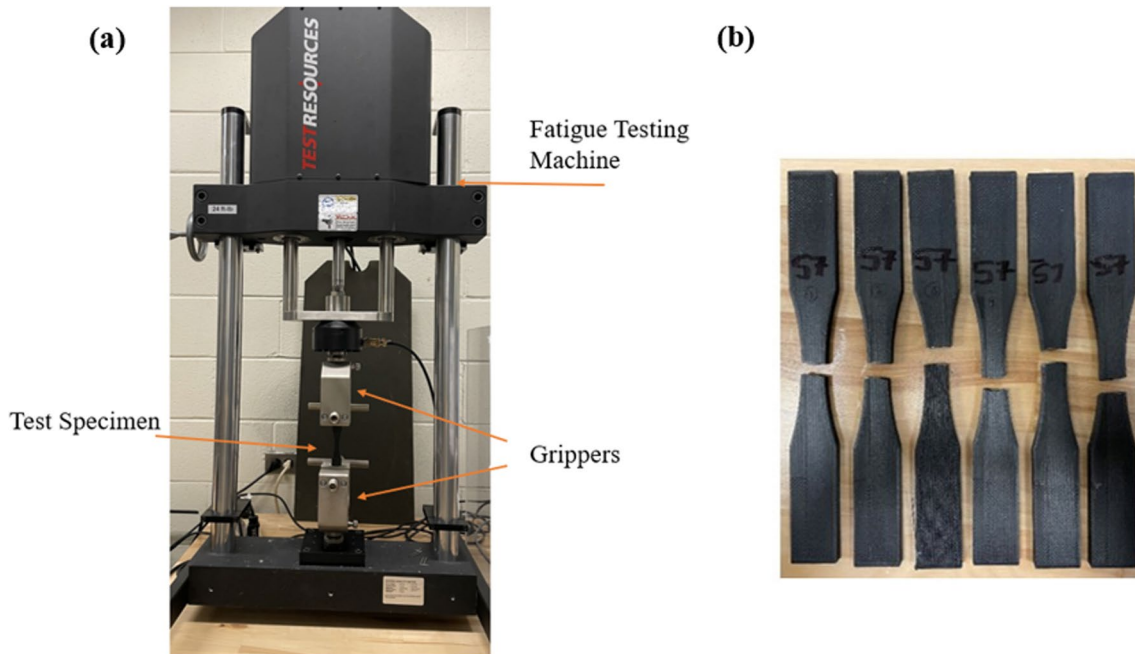
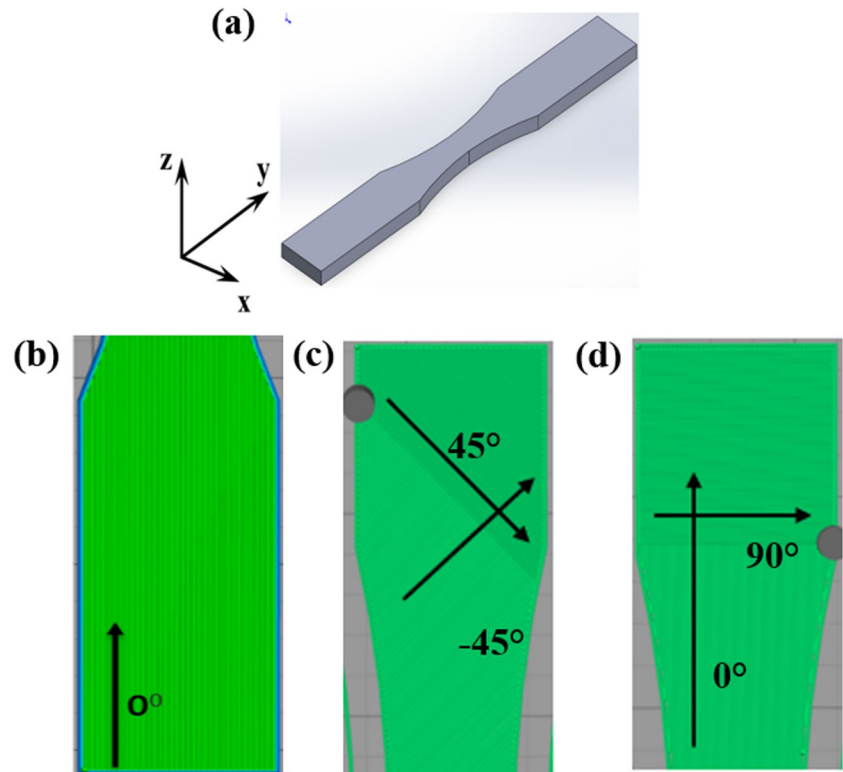


**Fig. 14** (a) Fatigue Testing Machine (b) Fractured specimens after fatigue testing

There are several ways in which laminates can affect the fatigue properties of the composites, such as the orientation of fibers, stacking sequence, thickness of laminates, etc. In this case, the stacking sequence, which also leads

to the orientation of fibers, has played a vital role. The unidirectional laminate, compared to angle ply and cross-ply laminates, has all of its fibers oriented in the same direction, which is the direction of maximum strength

**Table 5** Results of fatigue test for the type of laminates (Response – Number of cycles)

Specimen No	Unidirectional [0°] <sub>50</sub>	Angle-ply [45°/-45°] <sub>25</sub>	Cross-ply [0°/90°] <sub>25</sub>
1	362	25	21
2	644	23	38
3	176	10	58
4	888	17	82
5	504	28	53
6	816	15	78

[42]. This implies that the laminate is best able to resist fatigue loading in this direction. In angle-ply and cross-ply laminates, layers are oriented at different angles, which leads to the possibility of stress concentrations at the interfaces between the layers. These stress concentrations can be areas of weakness that steer to failure in fatigue loading conditions. Unidirectional laminates do not have these stress concentration areas leading to better fatigue performance. Additionally, since all the layers of unidirectional laminate are oriented in the same direction, it results in better adhesion between the layers and lesser defects in the printed parts.

### 3.2 Effect of layer heights

From the previous test results, unidirectional laminate [0°]<sub>50</sub> showed better fatigue results; therefore, it is continued for further studies, and layer heights are varied as 0.3, 0.2, 0.1- and 0.05-mm. Commercial filament (SCF weight percentage – 13.78%) is used to conduct this set of experiments. Except for layer height, all other printing parameters are

**Table 6** Kruskal–Wallis test summary for the type of laminates

Parameter	H-value	df	p-value
Type of Laminates	14	2	0.00912

**Table 7** Results of fatigue test for layer height (Response – Number of cycles)

Specimen No	0.3 mm	0.2 mm	0.1 mm	0.05 mm
1	30	362	982	3792
2	140	644	1384	3232
3	56	176	1074	3754
4	23	888	1194	2290
5	82	504	1024	2800
6	33	816	1232	2300

kept constant. The tests are carried out with constant stress conditions, i.e., 52 MPa maximum stress and 5.2 MPa minimum stress. The data obtained from the experimental results are shown in Table 7. The graphical representation of the results obtained is shown in Fig. 16. Statistical analysis was conducted on fatigue results to investigate the effect of layer heights, with the following hypotheses formulated: the null hypothesis states that the variance of layer heights does not have a significant impact on fatigue properties, while the alternative hypothesis proposes that the variation of layer heights has a statistical impact on fatigue properties.

As previously mentioned, the data's normality was assessed using the Shapiro–Wilk normality test, and the result generated a p-value of 0.010 with a significance level of 0.05, indicating that the data was not normally distributed. Additionally, the assumption of equal variances

**Fig. 15** The fatigue results in chart form for laminates

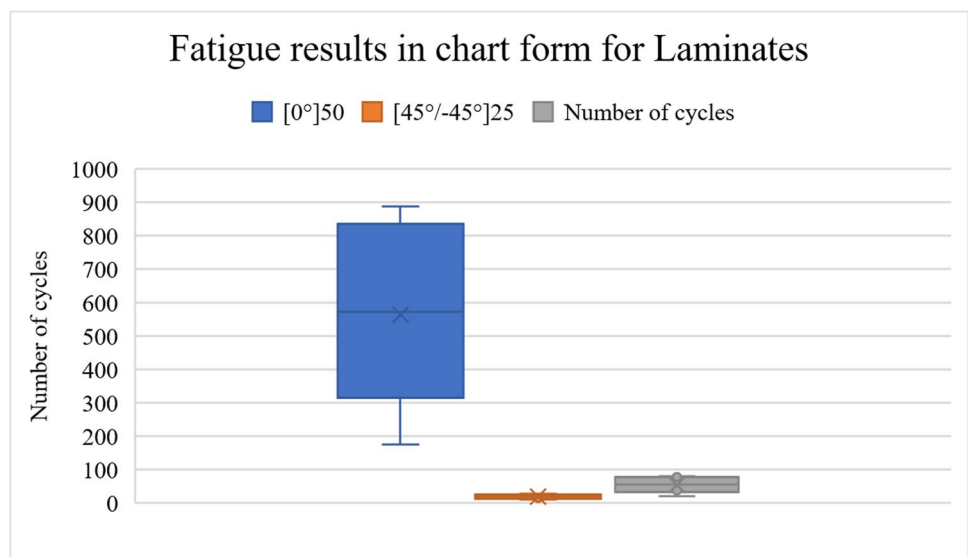


**Fig. 16** The fatigue results in chart form for layer heights

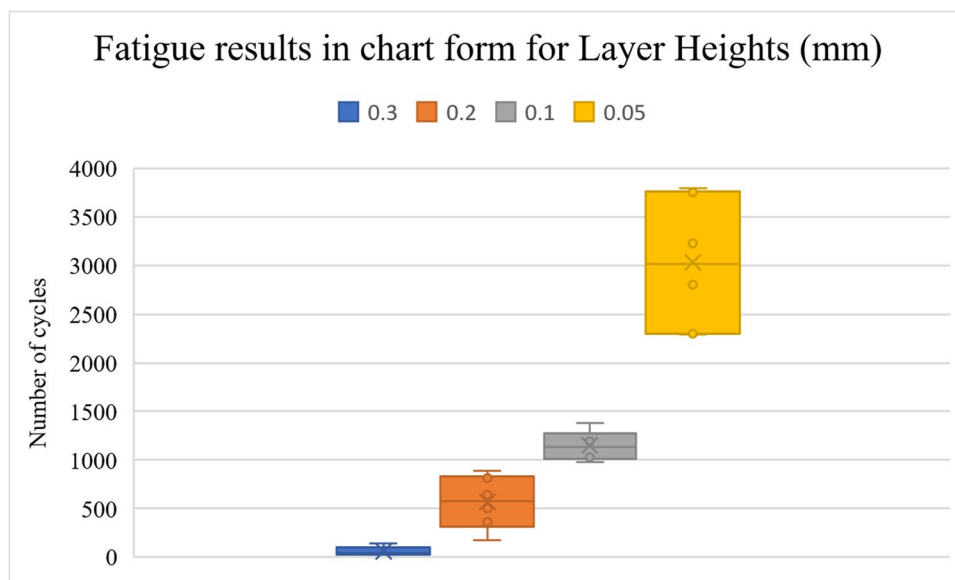


**Table 8** Kruskal–Wallis test summary for layer height

Parameter	H-value	df	p-value
Layer Heights	21.6	3	7.9E-05

was violated. Consequently, a non-parametric test, the Kruskal–Wallis method, was selected to analyze the data instead of ANOVA. Table 8 exhibits the Kruskal–Wallis test summary for the layer heights. The p-value for the variation in layer heights is less than 0.05, signifying strong evidence against the null hypothesis and indicating a significant difference between the groups. From Fig. 16 and Table 7, it is seen that the lowest output observed is 30–140 number of cycles for 0.3 mm layer height. For 0.05 mm layer height, the highest output is observed, i.e., range from 2290 to 3792. It can be concluded that the optimal layer height is 0.05 mm.

Reducing the layer height of a 3D-printed part can enhance the adhesion between adjacent layers of the material [43]. This is due to the fact that smaller layer heights increase the surface area of contact between each layer and the preceding one, thereby strengthening the bond. A decrease in layer height promotes favorable conditions for the subsequent layer to melt during contact with the hot extrudate on the previously printed layer. This process plays a crucial role in establishing interlayer adhesion [44]. Such improved bonding can boost the fatigue performance of the printed part. Reducing the layer thickness enhances the accuracy of the final product [43].

### 3.3 Effect of SCF Weight percentages

From the previous test results, as unidirectional laminate  $[0^\circ]_{50}$  and layer height 0.05 mm showed better fatigue life, it

**Table 9** Results of fatigue test for SCF weight percentage (Response – Number of cycles)

Specimen	Commercial Filament (13.78%)	Custom-made Filament (10%)	Custom-made Filament (16%)
1	3792	184	916
2	3232	582	210
3	3754	209	872
4	2290	392	387
5	2800	16	1176
6	2300	33	308

is continued for further studies, and SCF weight percentages are varied as mentioned earlier as 13.78% with commercial filament and 10 and 16% for custom-made filament. The rest of the parameters are kept constant. The tests are carried out with constant stress conditions, i.e., 52 MPa maximum stress and 5.2 MPa minimum stress. The data obtained from the experimental results is shown in Table 9. Figure 17 depicts the graphical representation of the obtained results. Statistical analysis was carried out on fatigue results to investigate the impact of carbon fiber weight percentage. The hypotheses tested were: Null hypothesis: Variation in carbon fiber weight percentage does not have a significant effect on fatigue properties. Alternative hypothesis: Variation in carbon fiber weight percentage has a statistical influence on fatigue properties.

Similar to the previous analysis, the Kruskal–Wallis method was used instead of ANOVA to analyze the data for this set of parameters. The Kruskal–Wallis test summary for the carbon fiber weight percentage is presented in Table 10, which shows that the p-value for the variation in SCF weight percentage is less than 0.05. The results provide substantial

**Fig. 17** The fatigue results in chart form for SCF weight percentages

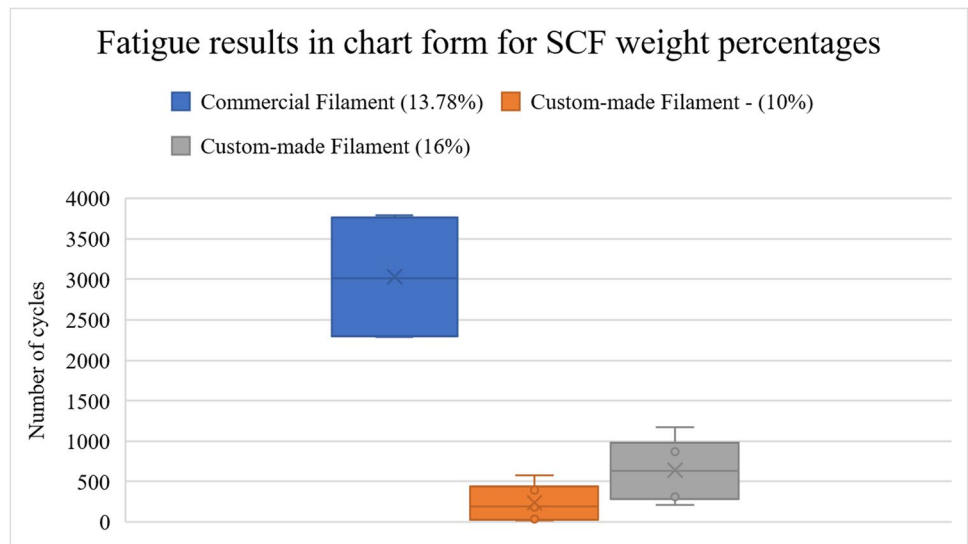


**Table 10** Kruskal–Wallis test summary for SCF weight percentage

Parameter	H-value	df	p-value
SCF weight percentages	13.05	2	0.001464

evidence to reject the null hypothesis and suggest that there is a significant difference between the groups. From Fig. 17 and Table 9, commercial filament (SCF—13.78%) performs better than custom-made filament with 10 and 16% SCF by weight. Though variation is more with a range of output from 2300 to 3792 number of cycles, commercial filament has the highest output. So, it can be concluded that the optimal carbon fiber weight percentage is 13.78% with commercial filament.

Increasing the weight percentage of SCF in composites generally leads to enhanced mechanical properties such as increased strength, toughness, and stiffness [45]. This can result in a longer fatigue life, as the material can better withstand cyclic loading without developing cracks or damage. As the weight percentage of SCF increases, there is an increase in load transfer between the matrix and the fibers, indicating that the fibers start to bear more load [10]. Nevertheless, there exists a trade-off between the weight percentage of carbon fiber and the composite’s performance to fatigue loading. With higher weight percentages of carbon fiber, the material leads to shorter fatigue life as it starts to accumulate in one place [9], which is called as percolation effect. The percolation effect is that when the system component or an index reaches a certain value (called the percolation threshold), some long-range associability will suddenly appear or disappear among the range of the percolation threshold, which makes the physical properties change sharply.

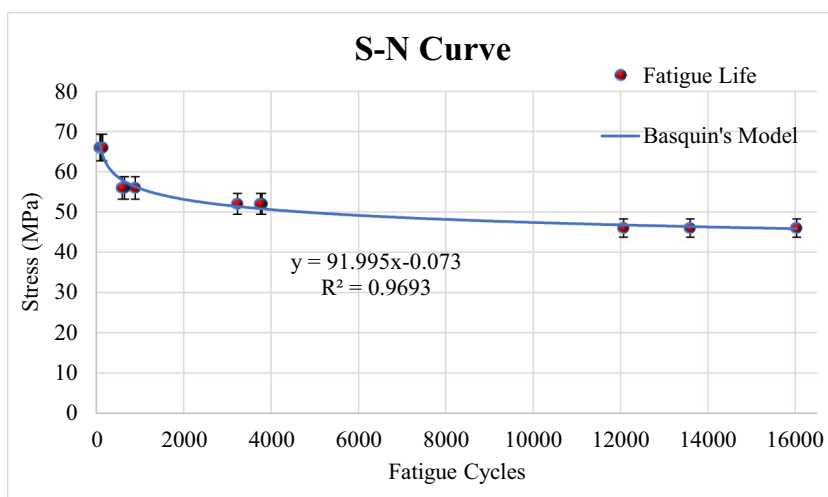
**Table 11** Result for Tensile Test (Commercial Filament, Layer height—0.05 mm, Unidirectional laminate [0°]<sub>50</sub>)

Specimen No	Ultimate Tensile Load (N)	Average Ultimate Load (N)	UTS (N/mm <sup>2</sup> )
1	3603	3552.66	71.05
2	3472		
3	3583		

### 3.4 S–N curve fitting

The optimal parameters from the selected process parameters are – Commercial Filament (SCF 13.78%), layer height—0.05 mm, and Unidirectional laminate [0°]<sub>50</sub>. With these parameters, more specimens are printed and tested at four stress levels, i.e., 95, 80, 75, and 65% of UTS. The UTS is determined by conducting static tensile tests with a strain rate of 5 mm/min on the three replicates of specimens, and then the average is taken as UTS. The result of tensile tests is presented in Table 11. The UTS is 71.05 N/mm<sup>2</sup> or MPa. For further simplification to give inputs for fatigue testing, it is considered 70 MPa, and 95, 80, 75, and 65% of 70 MPa are given as the maximum stress level inputs to the fatigue loading conditions. The S–N curve is plotted using the results obtained from the fatigue tests using Eq. (1), as shown in Fig. 18. The values for material constants A and b are 91.995 and -0.073, respectively. The data suggests that at higher stress levels, there is less variation in the results compared to lower stress levels. Additionally, all values at 95% of the ultimate tensile strength are below 150 cycles, indicating that the composite exhibits high susceptibility to failure. The highest number of cycles are found for the lowest stress level, i.e., 46 MPa, with a range from 12,069 to 16032. The higher value of R2 (0.9693) indicates that Basquin’s model provides a better fit to the data and is able to explain more of the variability in the data.

**Fig. 18** S–N curve fitted by Basquin's model



### 3.5 Fractographic analysis

The fracture zone for the carbon fiber reinforced specimen is depicted in Fig. 19 for commercial filament with a weight percentage of 13.78%. Figures 20 and 21 depict the fracture zone for the carbon fiber reinforced specimen for custom-made filament with a weight percentage of 10 and 16%, respectively. The SEM images show that for all the specimens, the fibers are pulled out and broken in the fracture zone. The fibers are the main carrier

of fatigue loading, and the matrix holds the fibers in position. Fiber breakage indicates that specimens are brittle in nature. In Figs. 20 and 21, there are voids present in the laminate, which could have been raised due to the under-extrusion. Under-extrusion happens when the diameter of the filament is less than the expected or set diameter as per printer specifications. Since these filaments are extruded in the laboratory and controlled manually, there is a possibility of variation in the diameter of the filament.

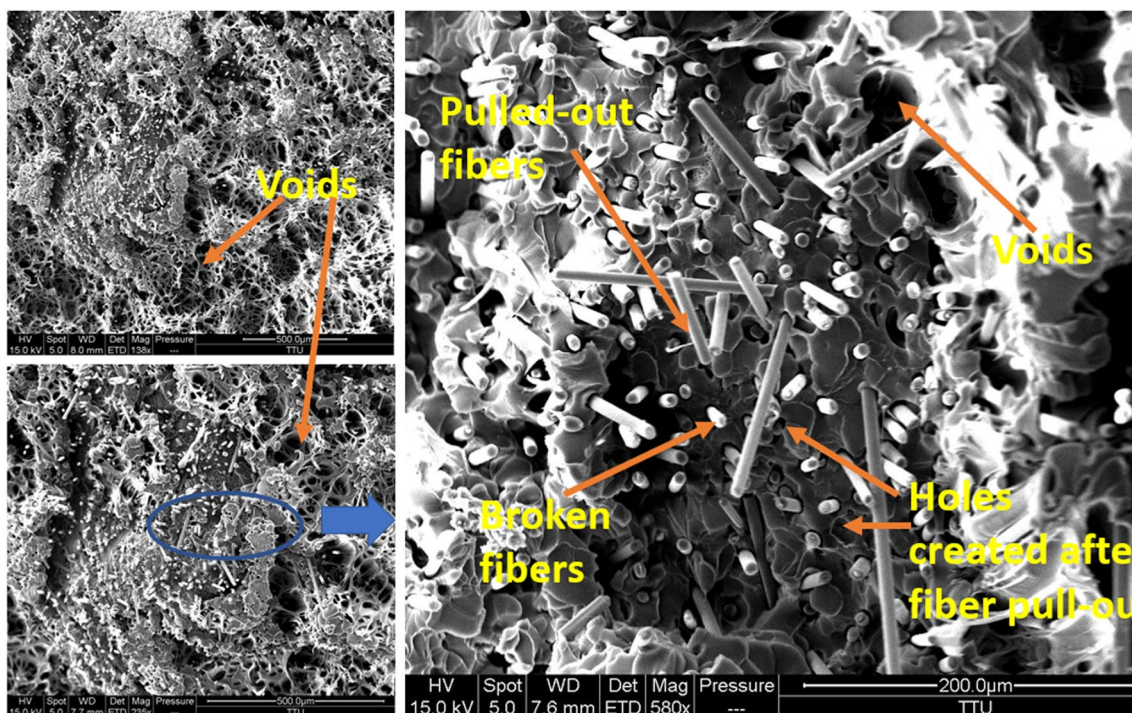


**Fig. 19** SEM images for fractured specimens of commercial filament (SCF 13.78% by weight, Layer height 0.05 mm, and Unidirectional laminate  $[0^\circ]_{50}$ )

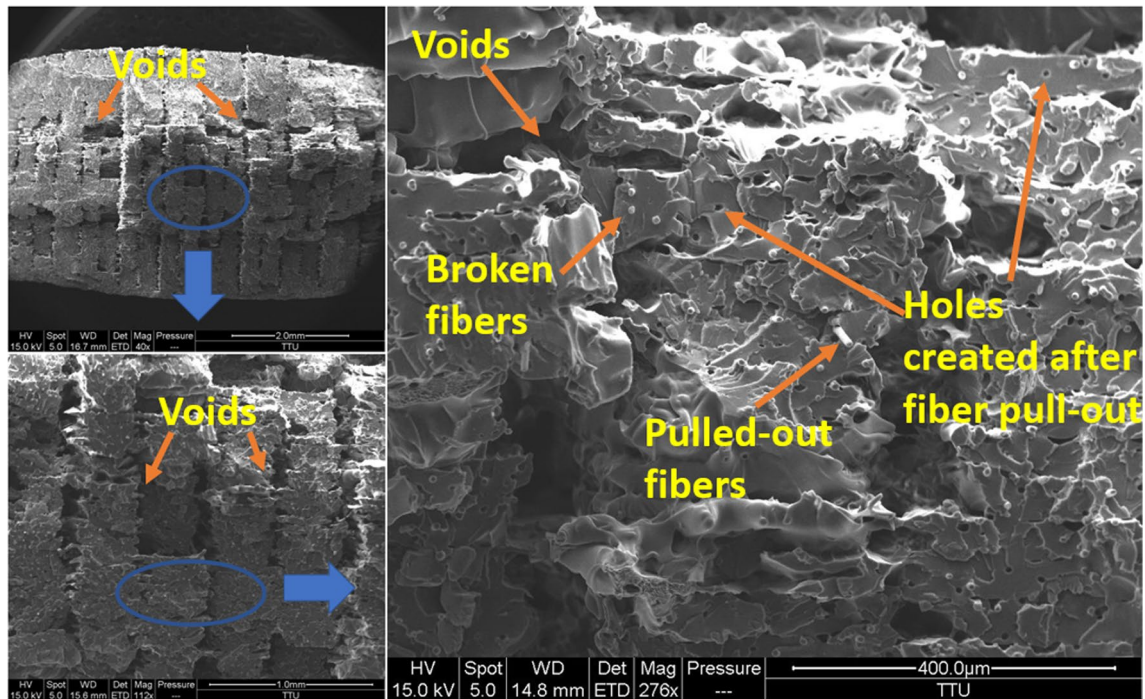


**Fig. 20** SEM images for fractured specimens of custom-made filament (SCF 10% by weight, Layer height 0.05 mm, and Unidirectional laminate  $[0^\circ]_{50}$ )

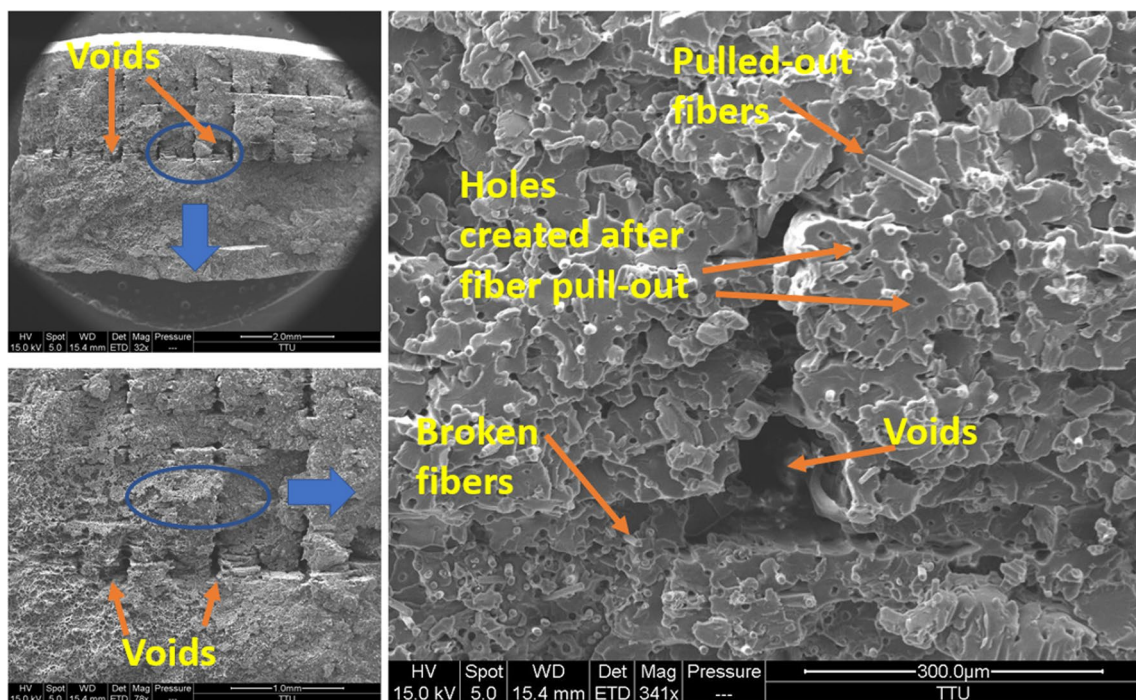


**Fig. 21** SEM images for fractured specimens of custom-made filament (SCF 16% by weight, Layer height 0.05 mm, and Unidirectional laminate  $[0^\circ]_{50}$ )

## 4 Conclusion

The present study provides a brief overview of additively manufactured CF-PETG composites using the MEX technique. The research delves into the fabrication process, fatigue characterization, and microstructural analysis of the specimens. Varying parameters taken into consideration are the type of laminates (unidirectional, angle-ply, and cross-ply), layer heights (0.3, 0.2, 0.1, and 0.05 mm), and carbon fiber weight percentages (13.78%, 10%, and 16%). In light of the results, the following conclusions can be reached:

- SCF is oriented in the extrusion direction when the composite filament is extruded three times. It plays a significant role in fatigue behavior.
- The type of laminates, layer height, and SCF weight percentage influence the fatigue life of SCF-PETG composites.
- Considering the type of laminates, unidirectional laminate  $[0^\circ]_{50}$  shows a better fatigue performance than angle-ply laminate  $[45^\circ/-45^\circ]_{25}$  and cross-ply laminate  $[0^\circ/90^\circ]_{25}$ .
- Decreasing the layer height aids in better adhesion, ultimately leading to better fatigue life of the composites. The reason behind this is that using smaller layer heights enhances the surface area of contact between each layer and the one before it. As a result, this strengthens the bond between the layers.
- Increasing the SCF weight percentage results in better fatigue until it reaches a value where SCF starts accumulating.
- Overall, from the parameters under consideration, the optimal parameters for the highest values of a number of cycles are commercial filament (SCF 13.78%), layer height—0.05 mm, and Unidirectional laminate  $[0^\circ]_{50}$ .
- Basquin's model is applicable to predict the fatigue life for SCF-PETG composite components manufactured by FFF.
- Microstructural analysis revealed that fibers are the main carrier of fatigue load, and it shows brittle behavior under fatigue. The voids present in the specimen are responsible for early failure under fatigue loading.

In the future, the prediction of fiber-reinforced composites should be considered. To verify the reliability of MEX regarding fatigue properties, it is essential to validate its performance on a range of different geometries or application-based components. By doing so, developing more generalized guidelines for the material's fatigue behavior will be possible.

**Acknowledgements** The authors want to thank Mr. Giovanni Mainardi and Wayne Hawkins at Tennessee Tech University, for their assistance in the experiments.

**Author contributions** All four authors contributed to various portions of the research project equally. Methodology, experimentation, and analysis were mostly done by Mithila Rajeshirke. The initial draft was written by Mithila Rajeshirke; revised, and finalised by Ismail Fidan, Orkhan Huseynov, and Suhas Alkunte. All the authors read and approved the final manuscript. The entire research project was managed by Ismail Fidan.

**Funding** This research has been funded by the Center for Manufacturing Research and the Department of Mechanical Engineering. The authors appreciate the provided funding.

## Declarations

**Conflicts of interest** The authors declare no conflict of interest.

## References

1. Dey A, Eagle INR, Yodo N (2021) A review on filament materials for fused filament fabrication. *J Manuf Mater Process* 5(3). <https://doi.org/10.3390/jmmp5030069>
2. "Additive manufacturing-General principles-Fundamentals and vocabulary 1,2." [Online]. Available: <https://www.iso.org/obp>. Accessed 05 Mar 2023
3. Ali MA, Fidan I, Tantawi K (2023) Investigation of the impact of power consumption, surface roughness, and part complexity in stereolithography and fused filament fabrication. *Int J Adv Manuf Technol* 126:2665–2676. <https://doi.org/10.1007/s00170-023-11279-3>
4. Hasanov S et al (2022) Review on additive manufacturing of multi-material parts: Progress and challenges. *J Manuf Mater Process* 6(1):4. <https://doi.org/10.3390/jmmp6010004>
5. Mohammadzadeh M, Lu H, Fidan I, Tantawi K, Gupta A, Hasanov S, Zhang Z, Alifui-Segbaya F, Rennie A (2020) Mechanical and thermal analyses of metal-PLA components fabricated by metal material extrusion. *Inventions* 5(3):44. <https://doi.org/10.3390/inventions5030044>
6. He F, Khan M (2021) Effects of printing parameters on the fatigue behaviour of 3d-printed abs under dynamic thermo-mechanical loads. *Polymers (Basel)* 13(14):1–23. <https://doi.org/10.3390/polym13142362>
7. Dolzyk G, Jung S (2019) Tensile and Fatigue Analysis of 3D-Printed Polyethylene Terephthalate Glycol. *J Fail Anal Prev* 19(2):511–518. <https://doi.org/10.1007/s11668-019-00631-z>
8. Padzi MM, Bazin MM, Muhamad WMW (2017) Fatigue Characteristics of 3D Printed Acrylonitrile Butadiene Styrene (ABS)". *IOP Conf Ser Mater Sci Eng* 269(1):012060. <https://doi.org/10.1088/1757-899X/269/1/012060>
9. Afrose MF, Masood SH, Iovenitti P, Nikzad M, Sbarski I (2016) Effects of part build orientations on fatigue behaviour of FDM-processed PLA material. *Progress Additive Manuf* 1(1–2):21–28. <https://doi.org/10.1007/s40964-015-0002-3>
10. Gupta A, Fidan I, Hasanov S, Nasirov A (2020) Processing, mechanical characterization, and micrography of 3D-printed short carbon fiber reinforced polycarbonate polymer matrix composite material. *Int J Adv Manuf Technol* 107(7–8):3185–3205. <https://doi.org/10.1007/s00170-020-05195-z>



11. Nasirov A, Gupta A, Hasanov S, Fidan I (2020) Three-scale asymptotic homogenization of short fiber reinforced additively manufactured polymer composites. *Compos B Eng* 202:108269. <https://doi.org/10.1016/j.compositesb.2020.108269>
12. Camargo JC, Machado AR, Almeida EC et al (2019) Mechanical properties of PLA-graphene filament for FDM 3D printing. *Int J Adv Manuf Technol* 103:2423–2443. <https://doi.org/10.1007/s00170-019-03532-5>
13. Imeri A, Fidan I (2020) Fatigue behaviors of fiber-reinforced composite 3D printing. *Fatigue Life Prediction of Composites and Composite Structures*. Woodhead Publishing 335–348. <https://doi.org/10.1016/B978-0-08-102575-8.00009-7>
14. Fidan I, Imeri A, Gupta A, Hasanov S, Nasirov A, Elliott A, Alifui-Segbaya F, Nanami N (2019) The trends and challenges of fiber reinforced additive manufacturing. *Int J Adv Manuf Technol* 102:1801–1818. <https://doi.org/10.1007/s00170-018-03269-7>
15. Andrzejewska A, Pejkowski L, Topoliński T (2019) Tensile and Fatigue Behavior of Additive Manufactured Polylactide. *3D Print Addit Manuf* 6(5):272–280. <https://doi.org/10.1089/3dp.2017.0154>
16. Imeri A, Fidan I, Allen M, Perry G (2018) Effect of Fiber Orientation in Fatigue Properties of FRAM Components. *Procedia Manuf* 26:892–899. <https://doi.org/10.1016/j.promfg.2018.07.115>
17. Imeri A, Fidan I, Allen M, Wilson DA, Canfield S (2018) Fatigue analysis of the fiber reinforced additively manufactured objects. *Int J Adv Manuf Technol* 98(9–12):2717–2724. <https://doi.org/10.1007/s00170-018-2398-7>
18. Pertuz-Comas AD, Díaz JG, Meneses-Duran OJ, Niño-Álvarez NY, León-Becerra J (2022) “Flexural Fatigue in a Polymer Matrix Composite Material Reinforced with Continuous Kevlar Fibers Fabricated by Additive Manufacturing. *Polymers* (Basel) 14(17):3586. <https://doi.org/10.3390/polym14173586>
19. Giannakis E, Koidis C, Kyratsis P, Tzetzis D (2019) Static and fatigue properties of 3D printed continuous carbon fiber nylon composites”. *Int J Modern Manuf Technol* XI(3):69–76
20. Pertuz AD, Díaz-Cardona S, González-Estrada OA (2020) Static and fatigue behaviour of continuous fibre reinforced thermoplastic composites manufactured by fused deposition modelling technique. *Int J Fatigue* 130:105275. <https://doi.org/10.1016/j.ijfatigue.2019.105275>
21. Antonio Travieso-Rodríguez J, Zandi MD, Jerez-Mesa R, Lluma-Fuentes J (2020) Fatigue behavior of PLA-wood composite manufactured by fused filament fabrication. *J Mater Res Technol* 9(4):8507–8516. <https://doi.org/10.1016/j.jmrt.2020.06.003>
22. Essassi K, lucRebiere J, El Mahi A, Ben Souf MA, Bouguecha A, Haddar M (2020) “Experimental and analytical investigation of the bending behaviour of 3D-printed bio-based sandwich structures composites with auxetic core under cyclic fatigue tests. *Compos Part A Appl Sci Manuf* 131:105775. <https://doi.org/10.1016/j.compositesa.2020.105775>
23. el Magri A, Vanaei S, Shirinbayan M, Vaudreuil S, Tcharkhtchi A (2021) An investigation to study the effect of process parameters on the strength and fatigue behavior of 3d-printed pla-graphene. *Polymers* (Basel) 13(19):3218. <https://doi.org/10.3390/polym13193218>
24. Ekoi EJ, Dickson AN, Dowling DP (2021) Investigating the fatigue and mechanical behaviour of 3D printed woven and non-woven continuous carbon fibre reinforced polymer (CFRP) composites. *Compos B Eng* 212:108704. <https://doi.org/10.1016/j.compositesb.2021.108704>
25. Nawafleh N et al (2020) Static and dynamic mechanical performance of short Kevlar fiber reinforced composites fabricated via direct ink writing. *J Mater Sci* 55(25):11284–11295. <https://doi.org/10.1007/s10853-020-04826-w>
26. Capela C, Oliveira SE, Ferreira JAM (2019) Fatigue behavior of short carbon fiber reinforced epoxy composites. *Compos B Eng* 164:191–197. <https://doi.org/10.1016/j.compositesb.2018.11.035>
27. Kováčová M et al (2020) Novel hybrid PETG composites for 3D printing”. *Applied Sciences* (Switzerland) 10(9):3062. <https://doi.org/10.3390/app10093062>
28. Bex GJP, Ingenhut BLJ, ten Cate T, Sezen M, Ozkoc G (2021) Sustainable approach to produce 3D-printed continuous carbon fiber composites: ‘A comparison of virgin and recycled PETG.’ *Polym Compos* 42(9):4253–4264. <https://doi.org/10.1002/pc.26143>
29. Latko-Durałek P, Dydek K, Boczkowska A (2019) Thermal, Rheological and Mechanical Properties of PETG/rPETG Blends. *J Polym Environ* 27(11):2600–2606. <https://doi.org/10.1007/s10924-019-01544-6>
30. Devsingh D, Dev AD, Avala B, Reddy R, Arjula S (2018) Characterization of additive manufactured petg and carbon fiber-petg static and dynamic analysis of centrifugal blower using composite material view project manufacturing and product analysis on composite frp pultruded products view project characterization of additive manufactured petg and carbon Fiber-PETG. *Int J Res Eng App Manag (IJREAM)* 04:2. <https://doi.org/10.18231/2454-9150.2018.0139>
31. Grzelak K et al (2021) Additive manufacturing of plastics used for protection against covid19—the influence of chemical disinfection by alcohol on the properties of abs and petg polymers. *Materials* 14(17):4283. <https://doi.org/10.3390/ma14174823>
32. Kumar KS, Soundararajan R, Shanthosh G, Saravanakumar P, Rattesh M (2021) Augmenting effect of infill density and annealing on mechanical properties of PETG and CFPETG composites fabricated by FDM. In *Materials Today: Proceedings*, Elsevier Ltd, 2186–2191. <https://doi.org/10.1016/j.matpr.2020.10.078>
33. Singh S, Singh R (2016) Development of functionally graded material by fused deposition modelling assisted investment casting. *J Manuf Process* 24:38–45. <https://doi.org/10.1016/j.jmapro.2016.06.002>
34. Mahesh V, Joseph AS, Mahesh V, Harursampath D, Chethan VN (2021) Investigation on the mechanical properties of additively manufactured PETG composites reinforced with OMMT nanoclay and carbon fibers. *Polym Compos* 42(5):2380–2395. <https://doi.org/10.1002/pc.25985>
35. “‘Pushplastic’”. [Online]. [https://cdn.shopify.com/s/files/1/0260/7421/files/PUSH\\_PLASTIC\\_CF\\_PETG\\_TDS.pdf?v=1624459432](https://cdn.shopify.com/s/files/1/0260/7421/files/PUSH_PLASTIC_CF_PETG_TDS.pdf?v=1624459432). Accessed: [01-Mar-2023].”
36. “‘compass.’” <https://compass.astm.org/document/?contentCode=ASTM%7CE1131-20%7Cen-US&proxycl=https%3A%2F%2Fsecure.astm.org&fromLogin=true> (accessed Mar. 14, 2023)
37. “‘3DXTech’”. [Online]. Available: <https://www.3dxtech.com/product/petg-pellets/>. [Accessed: 01-Mar-2023]”
38. “‘ZOLTEK’”, [Online]. Available: <https://zoltek.com/wp-content/uploads/2019/01/2021-PX35-Brochure.pdf>. Accessed [01-Mar-2023].”
39. “ISO 11782–1:1998 - Corrosion of metals and alloys — Corrosion fatigue testing — Part 1: Cycles to failure testing.” <https://www.iso.org/standard/1865.html> (accessed Jul. 19, 2023)
40. Alkunte S, Rajeshirke M, Fidan I et al (2023) Performance evaluation of fatigue behavior in extrusion-based functionally graded materials. *Int J Adv Manuf Technol*. <https://doi.org/10.1007/s00170-023-11922-z>
41. Huseynov O, Hasanov S, Fidan I (2023) Influence of the matrix material on the thermal properties of the short carbon fiber reinforced

- polymer composites manufactured by material extrusion. *J Manuf Process* 92:521–533. <https://doi.org/10.1016/j.jmapro.2023.02.055>
42. Kaw AK (2006) *Mechanics of composite materials*. Taylor & Francis
  43. Wu W, Geng P, Li G, Zhao D, Zhang H, Zhao J (2015) Influence of layer thickness and raster angle on the mechanical properties of 3D-printed PEEK and a comparative mechanical study between PEEK and ABS. *Materials* 8(9):5834–5846. <https://doi.org/10.3390/ma8095271>
  44. Rajeshirke M, Fidan I, Gupta A, Mäntyjärvi K (2022) Fatigue analysis of short carbon fiber reinforced composite components manufactured using fiber-reinforced additive manufacturing. In: 2022 International Solid Freeform Fabrication Symposium. <https://doi.org/10.26153/tsw/44139>
  45. Gay D, Hoa SV, Tsai SW (2003) *Composite materials : design and applications*. CRC Press
- Publisher's note** Springer Nature remains neutral with regard to jurisdictional claims in published maps and institutional affiliations.
- Springer Nature or its licensor (e.g. a society or other partner) holds exclusive rights to this article under a publishing agreement with the author(s) or other rightsholder(s); author self-archiving of the accepted manuscript version of this article is solely governed by the terms of such publishing agreement and applicable law.